D. H. Waldeck

Final Report for DOE Project DE-FG02-89ER14062

Title: *Experimental Studies of Photoinduced Charge Carrier Processes at Semiconductor-Electrolyte Interfaces*
PI: David H. Waldeck
Time Period: 1990 to 2000
Organization: Chemistry Department, 219 Parkman Avenue, University of Pittsburgh, Pittsburgh, PA 15260
Award: DE-FG02-89ER14062
Budget Status: No funds remain.

Research Summary Statement

This work has developed our fundamental understanding of the dynamical features of electron transduction and electron recombination at electrode interfaces, in particular, the semiconductor-electrolyte interface. Such understanding is essential to technological development because it illuminates the pathway for exercising a greater degree of control over these processes. Our studies have combined a wide range of techniques –electrochemical, optical spectroscopy, electron spectroscopy and theoretical modeling – to address these complex systems. We have pursued our studies on several fronts. Some of the primary accomplishments of this work are itemized below.

1. Our initial work aimed to develop time-resolved fluorescence spectroscopy as a tool for characterizing interfacial charge recombination. To this end we developed a quantitative understanding and modeling capability for the time-dependent bandgap emission of semiconductor electrodes immersed in electrolyte solutions. Our work clearly defined the important parameters to be considered for use of this technique, but also identified its weaknesses. It is now clear that this approach to studying the charge carrier dynamics at semiconductor interfaces is very useful because of its high time resolution, but is hampered by the system complexity and must be supported by other techniques.

2. A major component of our effort has been the development of surface coatings for semiconductor electrodes that stabilize them from corrosion and modify (either inhibit or accelerate) the rate of surface recombination. We developed approaches for coating surfaces of CdSe, InP and Si. The preparation of self-assembled monolayer films proved to be the most successful and has been used in performing a number of fundamental studies.

3. A component of our work has demonstrated that the self-assembly can be used to inhibit surface corrosion of InP and Ag. This demonstration is important for fundamental studies because the surface chemistry is controlled, but it may also be useful in a practical sense for improving the quality of corrosion inhibiting surface films on metals and semiconductors.

4. We have developed angle-resolved XPS and UPS capability to characterize the monolayer coated interfaces. These methods allow us to characterize a number of

DISCLAIMER

important aspects of the film-electrode interface, including its thickness, the nature of the bonding between the molecular moiety and the electrode, and the surface energetics.

5. A primary component of our effort has investigated the nature of electron tunneling through insulating barrier films to redox couples in solution. These studies have identified fundamental considerations for designing electron barriers that are 1 nanometer in size. In these studies we have shown that
   a) the presence of disorder in the molecular film causes a decrease in the electron transfer efficiency through the film. This observation is consistent with the known dependence of electronic coupling on molecular geometry for intramolecular systems.

   b) the dominant electronic coupling mechanism for electron transfer in covalent systems occurs through covalent bonding pathways of the films molecular constituents. In combination with this observation our work shows that ether linked molecular units have weaker couplings than methylene linked units because of quantum interference effects.

   c) the electronic coupling to redox species that are not covalently linked has a significant contribution from intermolecular electronic interactions within the film. This phenomenon is manifest by the different methylene chain length dependencies that are observed for electron transfer on Hg, Au and InP, for which the methylene chain's tilt angle and packing is different.

   d) we performed the first study of the transition between the weak coupling (electron tunneling) and strong coupling (adiabatic) regimes for the electron transfer and its dependence on monolayer film thickness.

6. We used AFM methods to characterize the island formation and growth mechanism for alkylsiloxane monolayer films on Si/SiO_x electrodes.

7. We performed a quantitative and comprehensive analysis of the photocurrent generation at InP electrodes. This allowed us to identify the bimolecular rate law, the rate law's transformation to first order for large redox couple concentration, and its subsequent transition to zeroth order with increasing light intensities. For high enough light intensities and film thicknesses the photocurrent was limited solely by the intrinsic tunneling rate.

8. Investigation of the electron tunneling in the absence of light was used to demonstrate the important role played by the voltage drop through the SAM layer, by its impact on the measured diode quality factor.

9. In collaboration with Prof. Ron Naaman (Weizmann Inst) we used low energy photoemission studies to demonstrate molecular manipulation of the interfacial electrostatic field for SAM coated electrodes. The nature of the electric field at the interface plays a critical role in electron transport. Through the use of low energy photoemission studies we were able to a) probe the shift in the interfacial field with the

size of the molecular dipole, b) investigate how molecular resonances modify the electron transport through the layer and c) study the dependence of electron transport on the organic films order.

Students and co-workers

Students who have worked on this project are

1. W. J. Dollard (PhD - 1993) – Employed at ICI Chemical Company.
2. M. L. Shumaker (PhD - 1993) – Chemistry Professor at Carlow College.
3. Y. Gu (PhD - 1999) – Employed at PSI Corp.
4. A. M. Sukharevsky (PhD 2000) Employed at Amgen
5. A. Napper (PhD expected in Fall 2001)
6. H. Yamamoto (PhD expected in Fall 2001)
7. Z. Lin (postdoc) – Employed at CoManage Corp.
8. H.Y. Liu (postdoc) – Employed at University of Pittsburgh

Undergraduate students who worked on these projects are D. Burdelski (graduate school at Harvard) and A. Bartko (graduate school at Georgia Tech)

Three African-American high school students worked on these projects through the Investing Now program at the University of Pittsburgh. Each of these students proceeded on to a technical or science program in college.

Publications

1 M. L. Shumaker, D. Burdelski and D. H. Waldeck, *"Time-Resolved Studies of Surface Recombination in CdSe Electrodes"*, in ***Picosecond and Femtosecond Spectroscopy from Laboratory to Real World,*** K. A. Nelson, ed. Vol. 1209 (SPIE, Bellingham, WA, 1990) 109-114.

2 M. L. Shumaker, W. J. Dollard, D. M. Zeglinski and D. H. Waldeck, *"Time-Resolved Fluorescence Studies of Chemically Derivatized CdSe Electrodes"*, ***Proceedings of the Society for Imaging Science and Technology***, (IS&T, Springfield, VA, 1991) 231-238.

3 M. L. Shumaker, W. J. Dollard and D. H. Waldeck, *"Carrier Relaxation at Semiconductor Interfaces and the Essential Features of a Quantitative Model"*, J. Phys. Chem. ***96*** (1992) 10371-10379.

4 W. J. Dollard, M. L. Shumaker and D. H. Waldeck, *"Time-Resolved Studies of Charge Carrier Relaxation in Chemically Modified Semiconductor Electrodes: n-CdSe/Silane Interfaces"*, J. Phys. Chem. ***97*** (1993) 4141-4148.

5 R. Tenne, K. Eherman, M. Peisach, W. Kautek, A. Wold, R. Matson, D. Mahalu and D. Waldeck, *"The WSe_2/Tungsten-Oxide Interface: Structure and Photoluminescence"*, Ber. Bunsenges. Phys. Chem. ***97*** (1993) 702-709.

6 D. H. Waldeck and D. N. Beratan, *"Molecular Electronics: Observation of Molecular Rectification"*, Science ***261*** (1993) 576-577.

7 A. Haran, D. H. Waldeck, R. Naaman, E. Moons and D. Cahen, *"The Dependence of Electron Transfer Efficiency on Conformational Order in Organic Monolayers"*, Science ***263*** (1994) 948-950.

8 K. H. Liao and D. H. Waldeck, *"A Photocapacitance Study of Chemically Sensitized TiO_2 Electrodes"*, J. Phys. Chem., ***99*** (1995) 4569 - 4576.

9 Y. Gu and D. H. Waldeck, *"Studies of Electron Tunneling at Semiconductor Electrodes"*, J. Phys. Chem. ***100*** (1996) 9573 - 9576.

10 Y. Gu, K. Kumar, Z. Lin, I. Read, M. B. Zimmt and D. H. Waldeck, *"Studies into the Character of Electronic Coupling in Electron Transfer Reactions"*, J. Photochem and Photobiol. A. ***105*** (1997) 189 - 196.

11 Y. Gu and D. H. Waldeck, *"Electron Tunneling at the Semiconductor-Insulator-Electrolyte Interface. Photocurrent Studies of the n-InP-Alkanethiol-Ferrocyanide System"*, J. Phys. Chem. B **102** (1998) 9015-9028.

12 Y. Gu, B. Akhremitchev, G. C. Walker and D. H. Waldeck, *"Structural Characterization and Electron Tunneling at the n-Si/SiO_2/SAM/Liquid Interface"*, J. Phys. Chem. B,**103** (1999) 5220-5226. Erratum, ibid, 5612.

13 H. Yamamoto, R. A. Butera, Y.-P. Gu and D. H. Waldeck, *"Characterization of the Surface to Thiol Bonding in Self-Assembled Monolayer Films on $C_{12}H_{25}SH$ on InP(100) by Angle-Resolved X-Ray Photoelectron Spectroscopy"*, Langmuir **15** (1999) 8640-8644.

14 K. Ray, A. Shanzer, D. H. Waldeck and R. Naaman, *"Resonances in Low-Energy Electron Transmission Through Organized Organic Films. Evidence for Molecular Quantum-Wells"*, Phys Rev. B **60** (1999) 13347-13350.

15 D. E. Khoshtariya, T. D. Dolidze, L. D. Zusman and D. H. Waldeck, "Turnover of the Solvent Friction (Overdamped) and Tunneling (Nonadiabatic) Charge Transfer Mechanisms for a Au/$Fe(CN)_6^{3-/4-}$ Electrode Process. Evidence for a Freezing Out of the Marcus Barrier", J. Phys. Chem. A (2001) ASAP.

16 A. M. Napper, H. Y. Liu, and D. H. Waldeck *"The Nature of Electronic Coupling between Ferrocene and Gold through Alkanethiolate Monolayers on Electrodes. The Importance of Chain Composition, Interchain Coupling, and Quantum Interference."* J. Phys. Chem. submitted (attached to report).

17 H. Yamamoto, H. Liu, and D. H Waldeck *"Immobilization of Cytochrome C at Au Electrodes by Association of a Pyridine Terminated SAM and the Heme of Cytochrome"* Chem. Commun.., submitted (attached to report).

February 10,2001

Immobilization of Cytochrome C at Au Electrodes by Association of a Pyridine Terminated SAM and the Heme of Cytochrome

Hiromichi Yamamoto, Haiying Liu, and David H Waldeck*
Department of Chemistry, University of Pittsburgh, Pittsburgh, Pennsylvania 15260

This work uses electrochemical methods to demonstrate that cytochrome c can be immobilized on electrodes that are coated with self-assembled monolayers of 4-pyridinyl-COO-$(CH_2)_n$-S (n > 6) through interaction between the pyridine terminal unit and the heme of the cytochrome

One avenue toward better sensors and enzyme electrodes is the use of a long tether, whose terminal functionality can selectively bind a biomolecule. Here this strategy is explored with the redox protein cytochrome c. Electron transfer reactions with cytochrome c have been extensively studied, both to clarify its function in biological systems and to provide a canonical example of a redox active protein[1]. Cytochrome c has been immobilized on COOH terminated self-assembled monolayers (SAMs) through electrostatic interactions between the carboxylate and the exterior of the protein[2] and by covalent linkage[3]. This work investigates the ligation between the terminal unit of the SAM, a pyridine, and the heme of horse heart cytochrome c. Raman and NMR studies have confirmed that the axial ligand (Met-80) of the cytochrome's heme can be displaced by an extrinsic ligand, such as CN^-, imidazole, or pyridine[4]. This work reports on the electron transfer and immobilization of cytochrome c on 4-pyridinyl-COO-$(CH_2)_n$-S (PyCOO-Cn, n = 2, 6, 11, 16) SAMs. The data show that immobilization of cytochrome is achieved by the pyridine functionality when the alkane tethers are long enough, n=6,11,16. In addition, the immobilization causes a large negative shift of the formal

potential E°' that does not occur for other immobilization strategies. The data also show that the electron transfer rate for the oxidation is enhanced over that for the reduction; i.e., an asymmetry in the electron transfer rates becomes evident. These data suggest that the pyridine interacts with the Fe^{3+} in the cytrochrome's heme.

The pyridine terminated SAM materials were constructed using a two part strategy. First the bis(ω-hydroxyalkanyl) disulfide was prepared from the ω-terminated hydroxyalkanethiols. Second, the pyridine derivatives of the disulfide were obtained through condensation with the 4-pyridinecarboxylic acid. The overall yield of the products were 76% for C2, 73% for C6, 75% for C11, and 74% for C16. The methylated pyridine, bis(6-hydroxyhexanyl) disulfide, was prepared by reflux of the pyridine disulfide in ethanol solution with excess iodomethane. See Supplemental Materials for further details.

The experiments used a three-electrode (Pt auxiliary, Ag/AgCl reference) electrochemical cell with a working electrode that was a Au ball (*ca* 1 mm diameter) to which the disulfide was self-assembled. Capacitance measurements were used to assess the quality of the SAM. For the immobilization studies the SAM coated electrodes were incubated in a cytochrome c solution and measurements were made in 25 mM phosphate buffer solution at pH 7. For the studies with OH terminated layers and PyCOO-C2, in which the cyt c is not immobilized, the purified cytochrome c was 30-50 μM in the buffer solution. See Supplemental Materials for further details.

Figures 1 show cyclic voltammograms for some of the systems that were studied. Panels A and B show voltammograms for SAMs that have pyridinal functionalities. The solid line curves show the electrode's response after it has been removed from the

incubation solution, rinsed, and placed in contact with a buffer/electrolyte solution that does not contain cytochrome c. The data in panel A shows no faradaic response for the buffer solution because cytochrome c does not adsorb onto the surface of PyCOO-C2, but does show a response when the electrode contacts a solution containing cytochrome c (dashed line). Panel B shows that some cytochrome adsorbs on the PyCOO-C11 SAM and displays a negative shift of the potential. A corresponding experiment using a SAM in which the pyridine nitrogen is blocked with a methyl group shows no faradaic current. Hence the adsorption of the cytochrome c requires that the nitrogen atom of the pyridine be accessible to the protein and the alkane chain be long enough. Panel C shows voltammograms for HO-terminated films[5], in contact with cytochrome c solution (dashed line). The solid line voltammogram is the same system with 0.8% pyridine (by volume) added to the solution. Two redox waves (apparent $E^{0'}$ of –17 mV and –325 mV) are found upon pyridine addition. The redox wave at –17 mV is assigned to the redox reaction of unmodified cytochrome c and the wave at –325 mV is assigned to the redox reaction of cytochrome c in which pyridine is coordinated to the heme. In this system, a positive potential sweep oxidizes the iron, and complexation with the pyridine occurs (or is strengthened). As the voltage is swept back negative the pyridine is not removed until the iron is reduced at the more negative reduction potential of the pyridine-coordinated moiety. To summarize, these data show that PyCOO-C11 SAMs immobilize cytochrome and cause an $E^{0'}$ shift that is consistent with an interaction between pyridine and the heme.

Analysis of the voltammetry data is presented in Table 1 for all of the systems studied. In each case the current-voltage curves were collected as a function of the

voltage scan rate. For the HO-C6 and PyCOO-C2 SAMs with cytochrome in solution, the peak current displayed a dependence on the square root of the scan rate, confirming that the cytochrome is not immobilized on the electrode surface. For the HOOC-C10 and the PyCOO-Cn (n=6,11,16) SAMs, the peak current was linear with the voltage scan rate, demonstrating that the cytochrome is immobilized on the surface. The apparent formal potential, E°', for the cytochrome immobilized on pyridine are significantly shifted from the other systems (see Table 1). The data for cytochrome immobilized on the PyCOO-C6, PyCOO-C11 and PyCOO–C16 SAMs show a negative shift of 150 to 160 mV from that found for the PyCOO-C2 system and from that of HOOC-C10. For the HOOC-Cn SAMs, the adsorption is attributed to electrostatic and hydrogen bonding interactions between the lysine groups ($-NH_3^+$) on the cytochrome c periphery and the carboxylic acid group of the SAM[2]. The negative shift of E°' suggests a different adsorption state for cytochrome on the pyridinyl layers than on the carboxylic acid layers and a significant interaction of the pyridine with the heme. The lack of adsorption and potential shift for the PyCOO-C2 SAM suggests that electrostatic and hydrogen-bonding interactions do not lead to adsorption, without significant deformation of the protein or the film. The nitrogen in the pyridinyl moiety of the SAM and the long alkyl chain are both needed for significant adsorption to occur.

Available literature results support the interpretation that the pyridine terminated SAMs coordinate to the heme. Recent Raman and NMR studies show that Met80, which is axially bound to the iron in the heme of cytochrome c, can be displaced by an imidazole or pyridine[4]. The apparent $E^{0'}$ values in the pyridine containing solution were found to be -17 and –325 mV, which is consistent with the reported result for yeast iso-1-

cytochrome c that complexes with imidazole[6]. Thus, the large negative shift of the $E^{0'}$ (342 mV) by pyridine in solution is caused by the axial ligand exchange from Met80 to pyridine on the heme's iron. The 10 to 20 mV shift in the $E^{0'}$ of the unsubstituted cytochrome is consistent with the change in solution dielectric constant caused by 1% pyridine[7]. These observations strongly suggest that the large shift of 150 to 160 mV in the PyCOOCn coated electrodes results from association of the pyridine with the heme. Although the amount of the shift observed on the SAM is about half of the shift found for the free pyridine, such a result is consistent with a reduced ability for optimal coordination when the pyridine is tethered to the SAM. Although a change in the local dielectric constant [7] or local field effects [8] may contribute to the potential shift, they are expected to be smaller than the shift observed here and show a chain length dependence.

The dependence of the voltammogram's peak position on the voltage scan rate can be used to quantify the electron transfer rate constant. For slow scan rates, the system remains reversible and the separation between the reduction and oxidation waves is fixed, but as the scan rate increases and exceeds the electron transfer rate the peak potentials shift. In short, the smaller the electron transfer rate, the larger the peak separation at a given scan rate. For the PyCOO-C6, -PyCOO-C11, and PyCOO-C16 SAMs the oxidation waves do not shift with increasing scan rate; *i.e.,* the rate remains too fast for the instrument to resolve. In contrast, the reduction peaks shift (see Table 1) and show a dependence on the alkane chain length of the SAM, reflecting the impact of the tunneling barrier thickness[9] on the electron transfer rate. This asymmetry in the transfer rate is consistent with stabilization of the heme by the pyridine. Such an interaction would enhance the oxidation rate and inhibit the reduction rate for which a dependence of

the peak position on the voltage scan rate is evident. The increase in the reduction peak's potential shift with scan rate as the alkane chain length increases reflects a slowing of the electron transfer rate because of an increased tunneling barrier width.

This study shows that cytochrome c can be immobilized on PyCOO-CnS SAMs with alkane chains of $n > 6$, and the adsorption occurs through association of the pyridine with the cytochrome's heme. This latter conclusion is supported by the large potential shifts, an induced asymmetry in the reduction and oxidation rates, and other literature results.

Acknowledgment

We are grateful to Prof. J. Shin and Dr. A. R. Lajmi for helpful advice. We acknowledge the Department of Energy for partial support of this work. We thank Hach Corporation for loan of the VoltaLab PGZ407 during part of this study.

Table 1. The apparent formal potential $E^{0'}$ and the change in peak potential between the high (20V/s) and low (0.1 V/s) scan rates.

	$E^{0'}$ (mV)[a]	$\Delta E_{p,ox}$ (mV)	$\Delta E_{p,red}$ (mV)
$PyCOO(CH_2)_2S$-	5	---	---
$PyCOO(CH_2)_6S$-	-159[a] ± 7	0	-11
$PyCOO(CH_2)_{11}S$-	-152[a] ± 5	0	-21
$PyCOO(CH_2)_{16}S$-	-147[a]	0	-44
$HO(CH_2)_6S$-	44 ± 2	---	---
$HOOC(CH_2)_{10}S$-	13 ± 3	32[b]	-24[b]

a – $E^{0'} = (E_{p,ox}+E_{p,red})/2$ at 100 mV/s scan rate and versus the Ag/AgCl reference.
b - Shift in the peak potential upon change in scan rate from 0.6 V/s to 10 V/s.

Figure caption

Cyclic voltammograms are shown for gold electrodes that are coated with A) 4-pyridinyl-COO-$(CH_2)_2$-S, B) 4-pyridinyl-COO-$(CH_2)_{11}$-S, and C) HO-$(CH_2)_6$-S SAMs. For Panel A, the solid line shows a voltammogram for an electrode that was incubated in 50μM cytochrome solution for 30 mins and placed in contact with a 25 mM buffer solution, and the dashed line shows the same electrode in contact with a 50 μM cytochrome c buffer solution. For Panel B, the solid line corresponds to the Py terminated layer after it was incubated in the cytochrome solution and the dashed line corresponds to a background curve. Panel C shows a voltammogram for cytochrome in a buffer solution (dashed line) and a voltammogram for a cytochrome solution containing 0.8% pyridine (solid line).

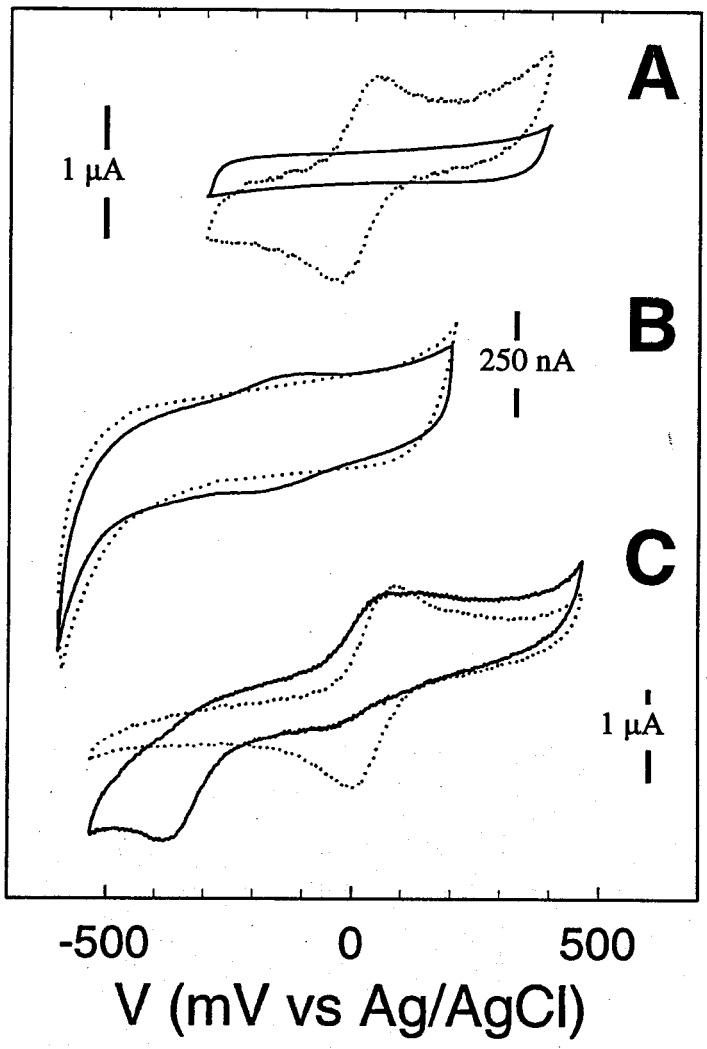

FIGURE 1

References

1 M. Fedurco, *Coord. Chem. Rev.* 2000, **209**, 263.

2 a) Tarlov, M. J.; Bowden, E. F. *J. Am. Chem. Soc.* 1991, **113**, 1847; b) Collinson, M.; Bowden, E. F.; Tarlov, M. J. *Langmuir*, 1992, **8**, 1247; c) Song, S.; Clark, R. A.; Bowden, E. F.; Tarlov, M. J. *J. Phys.Chem.* 1993, **97**, 6564.

3 C. J. McNeil, D. Athey, and H. Wo *Biosensors & Bioelectronics* 1995 **10** 75.

4 a) T. G. Spiro and X. Y. Li. Resonance Raman Spectra of Heme and Metalloproteins in Biological Applications of Raman spectroscopy; (Wiley, NY, 1988) **3**, 1; b) S. Hirota, T. Ogura, I. K. Shingawa, S. Yoshikawa, and T. Kitagawa *J. Phys. Chem.* 1996, **100**, 15274; c) S. R. Yeh, and D. L. Rousseau *J. Biol. Chem.* 1999, **274**, 17853; d) M. Smith and G. Mclendon. *J. Am. Chem. Soc.* 1981, **103**, 4912; e) J. C. Ferrer, J. G. Gullemette, R. Bogumil, S. C. Inglis, M. Smith, and A. G. Mauk. *J. Am. Chem. Soc.* 1993, **115**, 7507; f) G. Liu, Y. Chen, and W. Tang. *J. Chem. Soc., Dalton Trans.*, 1997, 795.

5 The cytochrome does not adsorb onto these films. See S. Terrettaz, J. Cheng, C. J. Miller, and R. D. Guiles *J. Am. Chem. Soc.* 1996, **118**, 7857.

6 B. A. Feinberg, X. Liu, M. D. Ryan, A. Schejter, C. Zhang, and E. Margoliash, B*iochemistry* 1998, **37**, 13091.

7 S. G. Sivakolundu and P. A. Mabrouk *J. Am. Chem. Soc.* 122, **2000**, 1513.

8 D. H. Murgida and P. Hildebrandt *J. Am. Chem. Soc.* 123, **2001**, ASAP.

9 H. Finklea, Electroanalytical Chemistry **19**, 109 (Marcel Dekker, NY, 1996).

The Nature of Electronic Coupling between Ferrocene and Gold through Alkanethiolate Monolayers on Electrodes. The Importance of Chain Composition, Interchain Coupling, and Quantum Interference.

Andrew M. Napper, Haiying Liu and David H. Waldeck*

Department of Chemistry, University of Pittsburgh, Pittsburgh, PA 15260.

ABSTRACT

Cyclic voltammetry was used to measure electron transfer rate constants of self-assembled mixed-monolayers on gold electrodes formed by coadsorption of a redox-active ferrocene-based alkanethiolate [$(\eta^5C_5H_5)Fe(\eta^5C_5H_4)CO_2(CH_2)_4X(CH_2)_6SH$, where X = $-CH_2-$ or -O-] and a diluent alkanethiolate [$CH_3(CH_2)_4Y(CH_2)_6SH$, where Y = $-CH_2-$ or -O-]. The replacement of a methylene link by an ether link in the redox-active component leads to a significant reduction in the rate of electron transfer. This originates from destructive interference between electron transfer pathways in the ether linked molecules. The corresponding replacement in the diluent leads to a smaller, but measurable, decrease in rate constant – suggesting that intermolecular electronic coupling pathways also contribute to the electron transfer.

INTRODUCTION

Electron transfer at interfaces is an area of great fundamental and practical importance. The creation of nanometer scale electronic materials is a new technology that relies on such processes. Understanding and controlling charge transport through organic films of nanometer thickness is of fundamental importance to this area of research and others (such as sensor technologies, anti-corrosion films, etc.). Knowledge of how chemical composition and chemical structure determine electron transfer between a solid substrate and a redox active molecule is central to the development of these applied areas of research. Recent studies show how phenomenological factors affect electron transfer at the interfaces, for example the solvent reorganization energy [1, 2], the density of electronic states in the metal [3, 4], and electronic coupling between the electrode and the redox couple [5, 6]. These studies explore the origin of one of these factors, the electronic coupling, in the properties of the molecules, which constitute the tunneling barrier.

The development of self-assembly methods for the construction of monolayer films on electrode surfaces provides a means to control and manipulate the interfacial characteristics [7]. This technology has been exploited to investigate fundamental issues of electron transfer between an electrode and a redox couple, either covalently attached or freely diffusing in solution [8,9]. When such films are composed of saturated molecules (most commonly alkanethiols), the film acts as a barrier to electron transfer from the electrode to a redox couple placed in solution. Through chemical synthesis the thickness of such films can be controlled to a precision of Ångströms. Numerous studies have investigated the thickness dependence of the electron transfer rate constant [8, 9,10] and find it to be well described by an exponential decay law of the type

$$k_{eT} \propto \exp(-\beta L) \qquad (1)$$

where β is an empirical parameter and L is the film thickness. For insulating films on metal electrodes, β is typically of the order of 1 $Å^{-1}$. Other systems, for example alkane films on InP [11] and films comprised of conjugated molecules [12], display weaker distance dependencies. Other studies have addressed the influence of temperature [13], solution composition [14], pressure [15], film heterogeneity [16] and double layer structure [14] on the transfer rate.

The perspective used to describe electron transfer through insulating films has been based on insights gained from studies of intramolecular and intermolecular electron transfer. For electron donor and electron acceptor units that interact weakly (the nonadiabatic limit), a superexchange mechanism [17, 18, 19, 20, 29] for the electronic coupling may be used successfully with molecular systems however its applicability to electron transmission through films is not well-established. The view that 'through-bond' superexchange coupling is dominant when it is a possible mechanism suggests that the electron transfer should be sensitive to the properties of the linking molecule (e.g., the alkane chain) such as its composition, connectivity, and geometry. In addition, it suggests that electron transfer through noncovalent interactions, which are present in the monolayer film, will be of minor importance. At a low level of approximation, this observation stands in contrast to the perspective of solid-state physics which views the electron transfer as occurring by tunneling through a barrier, a 'line-of-sight' mechanism. At a higher level of treatment these two views should be merged since the characteristics of the barrier are determined by the intramolecular and intermolecular properties of the film constituents. The current study investigates the importance of chain composition and interchain interactions (i.e., electronic coupling through nonbonded contacts) on the electron transfer rate constant for fully saturated chains.

The importance of film composition on the electron transfer rate is of current interest, in particular for building conductive links between electrodes ('molecular wires')

and for better insulating electrodes from one another. Miller and coworkers [21] studied the rate of electron transfer between a gold electrode and a freely diffusing redox couple in solution ($Fe(CN)_6^{2-/3-}$ and $Os^{III}(bipy)_3$) through self-assembled monolayers consisting of $HO(CH_2)_nX(CH_2)_mSH$, in which X denotes an ether, olefin or alkyne function. All three chemical modifications resulted in a decrease in the rate constant compared to the hydrocarbon parent ($X = CH_2$), by a factor of ca. 2. This result was interpreted to arise from a decrease in the electronic coupling across the monolayer. In contrast, Creager [22] has reported that an *n*-alkylcarboxamide linked ferrocene moiety has the same rate constant as an all *n*-alkane linked ferrocene. Finally, these results are distinct from studies of films comprised of fully conjugated molecules for which the conductivity is high [12,23].

Because of film compactness, interchain interactions can play a role in the electron transfer process [24,25,26]. Majda and coworkers [24] examined interchain electronic interactions by changing the tilt angle that thioalkanes make on the surface of a hanging drop mercury electrode. Upon tilting, the films retained their passivating character (indicating the absence of defects) as well as an increase in tunneling current ($Fe(CN)_6^{2-}$/ $Fe(CN)_6^{3-}$is the redox couple) as the tilt angle was increased. For a dodecanethiol film they found that the current increase could be fit to an exponential function with a β' parameter of 0.16 $Å^{-1}$. Although it represents a significantly weaker dependence than that found by changing the number of methylene units in the alkane chain, their result indicates an increase in electronic coupling $|V|$ as a result of enhanced chain-to-chain interaction. The authors estimated that chain-to-chain coupling was ca. 5 times smaller than through-chain coupling for alkylthiol monolayers. Finklea [25] examined monolayers containing the electroactive $HS(CH_2)_nC(O)NHCH_2pyRu(NH_3)_5^{2+/3+}$ and a diluent $HS(CH_2)_mCOOH$. This comprehensive investigation characterized both the reorganization energy, λ, and the

standard rate constant, k^0 for systems in which $m = n$ (matched) and $n > m$ (exposed). The matched systems displayed β values of 0.97 ± 0.03 per methylene, and the exposed systems displayed β values of 0.83 ± 0.03 per methylene – in reasonable agreement with other studies. For the systems in which $n < m$ (buried), β was a factor of 5-6 smaller, a value of 0.16 ± 0.02. This large drop in β suggests a strong effect of interchain coupling on the electron transfer. They suggest that this strong effect arises from the ability of the neighboring chains to form intermolecular hydrogen bonds between the terminal carboxylic acid group and the ruthenium redox couple. This result is in reasonable agreement with the recent work of Sek et al. [26] in which an increase in electron transfer rate is associated with internal hydrogen bonding between amide groups in the monolayer.

This study demonstrates the importance of chain composition and interchain effects for electron transfer in the four systems drawn in Figure 1. The rate constant for electron transfer to a ferrocene moiety that is tethered to an ether spacer is found to be 4-5 times smaller than that through a pure alkane chain. This reduction is found in films comprised of both an alkane diluent and an ether diluent, thereby muting possible concerns about subtle changes in the reorganization energy, or effective dielectric constant of the film. In addition, the comparison of electron transfer rates with a given electroactive system in differing diluent molecules demonstrates that interchain interactions have a ca. 33% effect on the electron transfer rate constant.

EXPERIMENTAL

Reagents. Dodecanethiol (98+%, Aldrich), Perchloric Acid (70%, Mallinkcrodt), Ethanol (200 proof, Pharmco Products, inc.), and Gold wire (99.99+%, 250μm dia., Goodfellow) were used as received. Water for preparing electrolyte solutions and rinsing of electrodes was purified using a Barnstead-Nanopure system and was 18MΩ cm. Thiourea (99%), potassium hydroxide, ferrocenecarboxylic acid (97%), 1,6-dibromohexane (98%), 1,5-pentanediol (99%), N,N'-dicyclohexylcarbodiimide (DCC), 4-(dimethylamino)pyridine (DMAP), sodium hydride (95%), 1-pentanol, and 12-bromo-1-dodecanol were purchased from Aldrich.

Electrode Fabrication. Gold wire was heated in a natural gas/O_2 flame to form a ball ca. 0.5 mm in radius. The exposed wire was sealed in a soft-glass capillary tube. The gold ball was re-heated in the flame until glowing and then cooled in a stream of Ar gas. The electrode was immediately placed into an ethanol solution of 1mM total thiol concentration. Typically a 9:1 molar ratio of diluent to electroactive thiol ratio comprised the deposition solution. Deposition time was typically 48 h following which the electrode was rinsed with copious quantities of absolute ethanol, followed by 18MΩ cm water. A brief (20 s) immersion in 40°C 1M $HClO_4$, prior to use in the electrochemical cell was found to improve the quality of the measured voltammograms.

Synthesis of $CH_3(CH_2)_4O(CH_2)_6SH$. 1-Pentanol (2.190 g, 24.84 mmol) was reacted with 95% NaH (0.753 g, 29.8 mmol) in dry tetrahydrofuran for 15 minutes. 1,6-dibromohexane (18.15 g, 74.55 mmol) was added, and the mixture was refluxed for three hours. After filtering the NaBr solid, the solvent was removed under vacuum. $Br(CH_2)_6O(CH_2)_4CH_3$ was obtained by column chromatography (silica gel, hexane and

dichloromethane, 1:1). 7-oxo-1-dodecyl mercaptan was prepared by converting the bromide to the mercaptan by treatment with thiourea followed by base hydrolysis and column chromatographic purification. ^{1}H NMR (300 MHz) $CDCl_3$: 3.399 (t, J = 6.75 Hz, 4H); 2.532 (q, J = 7.35 Hz, 2H); 1.605 (m, 4H); 1.422 - 1.265 (broad, 11H); 0.908 (t, J = 6.12 Hz, 3H).

Synthesis of $(\eta^5C_5H_5)Fe(\eta^5C_5H_4)CO_2(CH_2)_{12}SH$. 12-(Ferrocenylcarbonyloxy)dodecyl bromide was prepared as follows: DCC (0.9335 g, 4.52 mmol) was added to a concentrated solution of ferrocenecarboxylic acid (0.9541 g, 4.15 mmol), 12-bromo-1-dodecanol (1.0 g, 3.7 mmol) and DMAP (50.7 mg, 0.415 mmol) in dichloromethane at 0 ^{0}C. After 1 h the solution was allowed to warm to room temperature and was stirred overnight. After removal of the precipitated dicyclohexylurea (DCU) by filtration, the product was recovered by extraction with CH_2Cl_2. After washing the CH_2Cl_2 extracts twice with dilute HCl solution and water, it was dried over magnesium sulfate and evaporated under reduced pressure. The product was dissolved in methylene chloride and chromatographed on silica gel with methylene chloride. The bromide (a brown solid, 1.55 g) was obtained by evaporation under reduced pressure. ^{1}H NMR (300 MHz) $CDCl_3$: δ 4.814 (t, J = 1.86 Hz, 2H); 4.395 (t, J = 1.85 Hz, 2H); 4.216 (t, J = 6.6 Hz, 2H); 4.206 (s, 5H); 3.412 (t, J = 6.84 Hz, 2H); 1.857 (m, 2H), 1.730 (m, 2H); 1.42 (m, 4H); 1.398-1.297 (broad, 12H). A portion of this bromide (0.551 g, 1.15 mmol) and thiourea (0.263 g, 3.45 mmol) were added to 25 mL of absolute ethanol and the resulting solution was stirred and refluxed under argon overnight. After removal of solvent under vacuum, 25 mL of an aqueous solution of potassium hydroxide (0.193 g, 3.45 mmol) was added, and the mixture was refluxed for 4 h under argon and then cooled down to room temperature.

The resulting solution was extracted with three 50 mL portions of methylene chloride, and the combined extract was washed with dilute HCl solution and water, respectively. The extract was dried with anhydrous magnesium sulfate. The solution was concentrated under vacuum and chromatographed on silica gel with methylene chloride. The first yellow band contained the desired 12-(ferrocenylcarbonyloxy)dodecane thiol product (0.26 g, a brown solid), and a second yellow band contained the corresponding disulfide. ^{1}H NMR (300 MHz) $CDCl_3$: δ 4.812 (t, J = 1.86 Hz, 2H); 4.393 (t, J = 1.85 Hz, 2H); 4.214 (t, J = 6.6 Hz, 2H); 4.205 (s, 5H); 2.525 (q, J = 7.380 Hz, 2H); 1.707 (m, 2H), 1.609 (m, 2H); 1.435-1.288 (broad, 17H).

Synthesis of $(\eta^5C_5H_5)Fe(\eta^5C_5H_4)CO_2(CH_2)_5O(CH_2)_6SH$. A starting material, $HO(CH_2)_5O(CH_2)_6Br$ (12-bromo-6-oxo-1-dodecanol), was prepared by a procedure analogous to that used for $CH_3(CH_2)_4O(CH_2)_6Br$. ^{1}H NMR (300 MHz) $CDCl_3$: δ 3.622 (t, J= 5.88 Hz, 2H); 3.407 (m, 6H); 1.649 (m, 2H); 1.552 (m, 8H); 1.405 (m, 4H). 12-(Ferroceneylcarbonyloxy)-7-oxo-1-dodecyl mercaptan was prepared by a method analogous to that described above for the 12-(ferroceneylcarbonyloxy)dodecane thiol. ^{1}H NMR (300 MHz) $CDCl_3$: δ 4.802 (t, J = 1.91 Hz, 2H); 4.384 (t, J = 1.91 Hz, 2H), 4.217 (t, J = 6.54 Hz, 2H); 4.196 (s, 5H); 3.437 (t, J = 4.85 Hz, 2H); 3.404 (t, J = 5.00 Hz, 2H); 2.518 (q, J = 7.38 Hz, 2H); 1.752 (m, 2H); 1.613 (m, 8H); 1.386 (m, 5H).

Electrochemical Measurements. Cyclic voltammetry was performed using an EG&G PAR-283 potentiostat controlled by a PC running ver. 4.30 of PAR's M270 software and a GPIB board. All measurements were performed at room temperature. The counter electrode was a platinum spiral and potentials were referenced against a Ag/AgCl reference electrode from BAS.

BACKGROUND

The electron transfer rate constant. In the nonadiabatic limit, the electron transfer rate constant k_{eT} is given by the *Fermi Golden Rule* expression,

$$k_{eT} = \frac{2\pi}{\hbar}|V|^2 \, FCWDS \tag{2}$$

Equation 2 describes the rate of a nonadiabatic transition between two states, with an exchange interaction between the sites of magnitude $|V|$. *FCWDS* is the Franck-Condon Weighted Density of States and accounts for the impact of nuclear coordinates on the electron transfer rate. When $-\Delta G$ is smaller than the reorganization energy λ of the reaction (*normal region*) and high frequency vibrational modes of the donor and acceptor are not a significant part of the reorganization, the *FCWDS* may be written as

$$FCWDS = \frac{1}{\sqrt{4\pi\lambda k_B T}} \exp\left[-\frac{(\lambda + \Delta G)^2}{4\lambda k_B T}\right] \tag{3}$$

The reorganization energy, λ, consists of two components: an *inner sphere* contribution that is associated with internal coordinates of the redox species, λ_{in}, and an *outer sphere* component that is dominated by the solvent polarization, λ_{out}. For the ferrocene/ferrocenium redox couple, which is discussed here, a frequently used approximation is to consider only the dominant λ_{out} term. When the internal reorganization energy is important, a semi-classical expression for the rate constant should be used – however this level of sophistication is not needed for this study. See reference 27 for a more detailed discussion of this model.

For electron transfer at an electrode, eqs 2 and 3 must be generalized to consider the range of electronic states that are available in the solid. For an electron at energy E in the electrode, the free energy of reaction is given by

$$\Delta G = (E_F - E) + e\eta \tag{4}$$

where η is the overpotential and E_F is the Fermi level of the electrode. Substitution of eq 4 into eq 3 generates

$$k_{red}(E,\eta) = \frac{2\pi}{\hbar}|V|^2 \frac{1}{\sqrt{4\pi\lambda k_B T}} \exp\left[-\frac{((E_F - E) + e\eta)^2}{4\lambda k_B T}\right] \tag{5}$$

for transfer of an electron from a specific electrode energy state to an electron acceptor. The rate constant for reduction requires an integration over all energy states of the solid, so that

$$k_{red}(\eta) = \frac{2\pi}{\hbar}|V|^2 \frac{1}{\sqrt{4\pi\lambda k_B T}} \int_{-\infty}^{\infty} \rho(E) \exp\left[-\left(\frac{((E_F - E) + e\eta)^2}{4\lambda k_B T}\right)\right] f(E)\, dE \tag{6}$$

where $\rho(E)$ is the density of electronic states of the electrode (often an energy independent average value is used) and $f(E)$ is the Fermi-Dirac distribution law

$$f(E) = \frac{1}{1 + \exp[(E - E_F)/k_B T]} \tag{7}$$

An expression similar to eq 6 can be written for the oxidation current

$$k_{ox}(\eta) = \frac{2\pi}{\hbar}|V|^2 \frac{1}{\sqrt{4\pi\lambda k_B T}} \int_{-\infty}^{\infty} \rho(E) \exp\left[-\left(\frac{((E_F - E) - e\eta)^2}{4\lambda k_B T}\right)\right] [1 - f(E)] dE \tag{8}$$

Obtaining Rate Constants from Voltammograms. The electron transfer rate constants were obtained by measuring the peak shift as a function of scan rate in cyclic voltammetry experiments [28]. Working curves of log(scan rate) vs. peak position were generated for specific values of λ and T by a Microsoft QuickBasic routine which

numerically integrated the relevant equations. These working curves were used to fit the experimental data.

Equations 6 and 8 were modified to calculate synthetic cyclic voltammograms. In particular, the electronic density of states in the metal was approximated as being constant over the energy regime that contributes significantly to the measured current. In this case eqs 6 and 8 become

$$k_{\mathrm{red},\eta} = \mu\rho k_B T \int_{-\infty}^{\infty} \frac{\exp\left[-\left(x - \frac{(\lambda+\eta)^2}{k_B T}\right)\left(\frac{k_B T}{4\lambda}\right)\right]}{1+\exp(x)} dx \tag{9}$$

$$k_{\mathrm{ox},\eta} = \mu\rho k_B T \int_{-\infty}^{\infty} \frac{\exp\left[-\left(x - \frac{(\lambda-\eta)^2}{k_B T}\right)\left(\frac{k_B T}{4\lambda}\right)\right]}{1+\exp(x)} dx \tag{10}$$

in which x is $(E_F - E)$, μ is a parameter that contains the distance dependent electronic coupling between the electrode and molecule, and ρ is the effective density of electronic states in the metal electrode. The integrals were evaluated numerically, from -9 to +9 V at a step size of 1 mV using Simpson's rule.

The measured current i_{meas} in the voltammetric experiment is directly related to the reduction and oxidation rate constants [28]. The linear sweep voltammograms were generated by application of eqs 11 and 12, using a potential step size of 0.5 mV. The dimensionless current i_{norm} may be written as

$$i_{\mathrm{dimensionless}} = \frac{\Delta f}{\Delta E/(RT/F)} = \left(\frac{RT/F}{\Delta E}\right)\left(f_{\mathrm{target}} - f_{\mathrm{initial}}\right)\left(1 - \exp\left[-\left(k_{\mathrm{red}} - k_{\mathrm{ox}}\right)\Delta t\right]\right) \tag{11}$$

$$f_{\mathrm{target}} = \frac{1}{1+\exp(-EF/RT)} \tag{12}$$

in which Δt is the time interval over which the potential is applied ($\Delta t = \Delta E / \nu$), ν is the sweep rate, ΔE the potential step size, and f_o is the fraction of oxidized species initially present in the time interval over which the potential step is applied.

Working curves of log (ν / k) vs. peak position ($E_p - E^0$) were generated and used to fit the experimental data. For a fixed standard rate constant, Figure 2 demonstrates the increasing deviation of the curve maxima from the fully reversible value of E^0. This change arises from the inability of the electron transfer event to keep up with the rapidly scanning sweep rate. The peak shape and movement away from a thermodynamic value of $E^0(\nu \rightarrow 0)$ is a kinetic effect. Note the broadening of the curve and the decrease in peak height at higher values of log(ν / k). At low sweep rates, the curve width at half height is equal to the thermodynamic value of 90.6 mV (at 298 K). $k_{ox,0}$ and $k_{red,0}$ were set to 5 s^{-1} in the simulation, by alteration of the prefactor $\mu\rho k_B T$ in eq 9.

RESULTS

The quality of the electroactive SAMs was assessed by three factors: peak widths at low scan rate, peak separations at low scan rates, and fractional ferrocene coverage. Typically, the peak widths were between 90 and 110 mV for the slowest scan rates. For an ideal system at thermodynamic equilibrium, the peak width is expected to be 91 mV [8]. Figure 3 shows a voltammogram for an ether-linked ferrocene in an alkane diluent at an intermediate scan rate. As the scan rate is lowered the peak separation decreases toward zero, indicating ideal thermodynamic behavior. Surface coverage of the ferrocene was estimated from the integrated charge of the ferrocene/ferrocenium species and the electrode's physical surface area, which was estimated by measuring the diameter of the gold balls with calipers. Typical ferrocene coverages were between 5% and 15%.

Figure 4 presents plots of the peak-to-peak separation between the oxidation and reduction waves of the voltammogram for each of the four systems. The more rapid increase in the peak separation for the ether-linked ferrocene (open triangles are ether diluent and the filled triangles are for alkane diluent) as compared to the alkane-linked ferrocene (open squares are for the ether diluent and the filled squares are for the alkane diluent) is clearly evident. In each case a best fit of the rate constant to the model (eqs 9-12) is shown. It is evident that the model for the rate constant characterizes the dependence well. The standard rate constant, k^0, values that are obtained from these fits are reported in Table 1.

Figure 5 illustrates how the assumed λ affects the quality of the data fitting. The solid line represents a fit to $k^0 = 52.8\ s^{-1}$ and $\lambda = 0.8$ eV. The dashed lines represent fits with $k^0 = 52.8\ s^{-1}$ and $\lambda = 0.6$ or 1.0 eV. A 25% change in λ does not seem to compromise the quality of fit significantly. Presumably any small difference in λ between the four systems does not significantly alter the calculated rate constants.

The best fit rate constants are provided in Table 1. The introduction of an ether linkage into the electroactive thiol chain has a dramatic effect upon the rate constant,

causing a reduction of 4.2 to 4.5 times. This observation is consistent with 'through-bond' electronic coupling of the ferrocene/ferrocenium with the electrode. A similar reduction in rate constant is found for both the ether and the alkane diluent and suggests that changes in the reorganization energy that one might find upon replacing the methylene in the alkane with an oxygen atom (the ether) is not the origin of this affect. A comparison of the same electroactive tether in the two different diluents (ether and alkane) reveals a much smaller, but still quite visible, change in the rate constant. For both electroactive species the electron transfer rate constant is smaller in the ether diluent and by a similar amount (30% and 36% reductions), even though the absolute rate constants differ by a factor of 4 to 5 for the two types of electroactive tethers.

DISCUSSION

The superexchange mechanism, first proposed by McConnell in 1961 [29], to explain the electron exchange in α,ω-diphenylalkane anions, is a perturbation treatment for the electronic interaction between molecular subunits. In this treatment the expression for $|V|$ is given by

$$|V| = \frac{H_{01}H_{n-1,n}}{(E-E_1)}\left(\prod_{i=1}^{n-1}\frac{H_{i,i+1}}{E-E_{i+1}}\right) \qquad (13)$$

in which n is the number of bridge sites, $H_{i,i+1}$ represents the exchange integral between adjacent bridge sites, and E is the electronic energy at which the electron tunnels from the donor to the acceptor. For identical bridge units, the product in eq 13 can be replaced by $(t / \Delta)^{n-1}$ where t is the exchange coupling between adjacent bridge units and Δ is the energy difference between the bridge sites and the tunneling energy. For long bridges, $|V|$ behaves approximately as an exponentially decaying function, so that

$$|V| = |V_0|\exp[-\beta(n-n_0)] \quad ; \quad \beta = -\ln\left(\left|\frac{t}{\Delta}\right|\right) \qquad (14)$$

in which $|V_0|$ would be the coupling in the absence of a bridge and β is the exponential decay parameter (see eq 1). Replacement of one of the bridging methylene units by an oxygen atom introduces two different exchange integrals (t for the methylene and t' for the ether link) in eq 13 and modifies the denominator accordingly (Δ for the methylene and Δ' for the ether link). One expects the rate constants to differ by the factor

$$\frac{k_{\mathrm{eT,\,alkane}}}{k_{\mathrm{eT,\,ether}}} = \frac{t^4}{t'^4}\frac{\Delta'^2}{\Delta^2} \qquad (15)$$

This development of superexchange relies on the nearest-neighbor (tight binding) interactions in order to calculate the electronic coupling through a bridge unit. It has been shown for long bridges that the nearest neighbor coupling is not the dominant coupling mechanism. Indeed, the majority of the interaction arises from pathways that skip over some bonds. If non-nearest-neighbor interactions are considered, many more pathways have to be considered; all of which contribute to the total electronic coupling. By calculating V with the appropriate phase factor, it is possible to calculate electronic couplings for all possible routes through a molecule. The total electronic coupling is equal to the sum of the contributions from each specific pathway. It is also possible that the different pathways will have different phases and result in destructive interference. In this case, the total electronic coupling will be smaller than that obtained by summing the magnitude of the couplings for each path, ignoring the phase term.

A pathway analysis was conducted on two model compounds: $^{\bullet}CH_2(CH_2)_{11}CH_2^{\bullet}$ and $^{\bullet}CH_2(CH_2)_5O(CH_2)_5CH_2^{\bullet}$. The geometry of the triplet diradical was optimized at the UHF/3-21G level of theory using Gaussian 98[30]. Previous studies show that this level of theory gives reasonable results [31]. The canonical Molecular Orbitals were transformed into the Natural Bond Orbital [30b] (NBO) basis. The α-spin bonding and antibonding NBOs (as well as the two lone pairs on the oxygen) were extracted and analyzed in two different ways.

First, the Fock matrices corresponding to the bonding manifold in the two diradicals were diagonalized, and the energy splitting of the HOMO and HOMO-1 levels was taken as being equal to 2 $|V|$. Although the same analysis was also performed using the antibonding manifold, it was found to contribute a much smaller electronic coupling and was ignored in the proceeding pathway analysis. The results of the Fock-matrix diagonalization procedure are presented in Table 2. The electronic coupling from the Fock-matrix diagonalization procedure is ca. 85% larger for the all methylene diradical than in the dihexyl ether diradical. A similar result was observed by Miller et al. [21]

who examined $^{\bullet}CH_2(CH_2)_7CH_2^{\bullet}$ and $^{\bullet}CH_2(CH_2)_3O(CH_2)_3CH_2^{\bullet}$ and observed a 51% increase in the coupling for the all methylene case relative to the ether compound. Miller ascribed the decrease in $|V|$ for the ether compound to the poor orbital overlap between the methylene bridging units and the oxygen.

Second, a pathway analysis of the bonding orbital manifold in both model compounds was performed. The pathways through the σ manifold were used since the coupling through the σ^* manifold was found to be so much weaker. A program was written that calculated all possible (forward hopping) pathways through the two model diradicals using the NBOs corresponding to the free radical on the terminal carbons and the sigma bonding orbitals along the backbone. In addition, the lone pairs of electrons on the oxygen in the ether diradicals were incorporated. Routes through the carbon (and oxygen) backbone were considered, leading to the couplings presented in Table 3. The program was extended to consider routes through C-H bonds in addition to routes through the backbone. This calculation was computationally much more intensive, but gave similar results.

Figures 6 and 7 illustrate the four routes that contribute the greatest to the overall electronic coupling. It is clear from these figures and the coupling magnitudes that the nearest neighbor pathway is no more significant than pathways that involve non-nearest neighbor couplings. For the ether linkages, there are many pathways with an opposite phase. Because the total coupling is a sum over all of the pathways, the terms of opposite sign cancel, leading to a decrease in the overall electronic coupling. In contrast, all of the pathways for the alkane system have the same sign. It seems that the main reason for the decrease in coupling between the methylene and ether linkers arises from the introduction of *destructive interference amongst pathways.* Table 3 presents these results in more detail, in particular the total coupling, the in-phase contributions, the out-of-phase contributions and the sum of the 'unsigned' couplings, for both systems. When the sum of the pathways is taken without regard to the sign of the coupling the two values of $|V|$

are within 10% of each other. When the sum is taken with consideration of the sign, the total coupling for the ether linked system is significantly smaller and in reasonable agreement with the experimental change in the rate constant (note that k_{eT} is proportional to $|V|^2$). The affect of adjacent chains were not taken into account in these calculations.

This result is in qualitative agreement with earlier studies for intramolecular electron transfer systems. Previous studies have shown that the efficiency of pure methylene chains in mediating the electron transfer process is superior to that of saturated ring systems. A β of 0.34 per methylene has been calculated [31f] as the limiting value ($m > 10$) for molecules of the type: CH_2=CH-$(CH_2)_m$-CH=CH_2. Bridges of comparable length with cyclobutane or norborane units have been shown [31f] to have a larger value of β (and smaller electronic coupling), and its origin lies with the introduction of pathways that destructively interfere.

These electrochemical rate data show that the through bond interaction is stronger than the inter-chain interaction for the ferrocene tethered systems. Nevertheless it is evident that changing the chemical composition of the diluent chains has a noticeable effect upon the rate of electron transfer. A reduction of approximately one-third is found upon going from an alkane diluent to an ether containing diluent, and both pairs A/A & A/O and O/A & O/O show a similar reduction in rate constant going from alkane to ether linked diluents. It is reasonable to expect that the intermolecular interactions will be more important for systems in which the redox couple is not covalently linked to the insulating film.

Equation 2 predicts that the rate constant is proportional to the square of the electronic coupling matrix element. Assuming that the Franck-Condon Weighted Density of States is similar for both systems, the ratio of experimental rate constants can be used to determine the relative ratio of electronic couplings in the alkane and ether linked systems. By comparing the A/A and O/O systems, the ratio of rate constants is 55.0/8.4 or 6.5, so presumably the ratio of V_{alkane} / V_{ether} should be equal to the square root of this

quotient, or 2.5. Using the data obtained from diagonalizing the reduced NBO Fock matrix, the value calculated is 0.7215 / 0.3910 = 1.845. Comparing the pathway calculations leads to a calculated value of 0.1979 / 0.1145 = 1.728. The theoretical values agree reasonably well with experiment, which seems to confirm the validity of the model compounds being used to draw conclusions about the ferrocene tethered systems.

CONCLUSIONS

The replacement of a single methylene group by an ether link in the electroactive thiol causes a marked decrease in rate constant. This result arises from a decrease in electronic coupling between the gold surface and ferrocene redox couple. A pathway analysis shows that the decrease in coupling arises from the presence of interfering pathways in the ether linked molecule. Also, the introduction of an ether linkage in the diluent thiols led to the observation of a reduced rate constant. This latter result is suggestive of the importance of intermolecular interactions when determining the electronic coupling through compact films.

ACKNOWLEDGMENTS

This research was supported by the US Dept of Energy, Division of Chemical Sciences (Grant #DE-FG02-89ER14062). We would like to thank Prof. K. D. Jordan and Prof. D. N. Beratan for useful discussions during this study.

FIGURE CAPTIONS

Figure 1. Schematic illustration of the four systems studied.

Figure 2. Synthetic linear sweep voltammograms were generated for the following $\log(\nu / k^0)$ parameters: A = -2.0, B = -1.0, C = 0, D = 1.0, E = 2.0, F = 3.0. A value of 5.0 s^{-1} was chosen for k^0.

Figure 3. This figure shows a typical cyclic voltammogram for the O/A system, at a scan rate of 3200 mV/s.

Figure 4. Plot of $(E_p\text{-}E^0)$ vs. log (sweep rate) for all four systems studied. The solid lines are the best fit to the data points using the Marcus model described in the text. λ is taken to be 0.8 eV and T = 298 K. The data points are from a specific run, and the calculated k^0 is 52.8 s^{-1} for A/A (filled squares) 37.3 s^{-1} for A/O (open squares), 12.2 s^{-1} for O/A (filled triangles), and 4.4 s^{-1} for O/O (open triangles).

Figure 5. This figure shows fits to the peak separation data for A/A using different values of the reorganization energy. The dotted lines show the fits of the rate data to reorganization energies of 0.6 and 1.0 eV at a fixed rate constant of 52.8 s^{-1}.

Figure 6. The four dominant pathways for the all methylene diradical model compound are shown, along with the contribution each one makes to the electronic coupling.

Figure 7. The four dominant pathways for the ether linked diradical model compound are shown, along with the contribution each one makes to the electronic coupling.

1. A/A

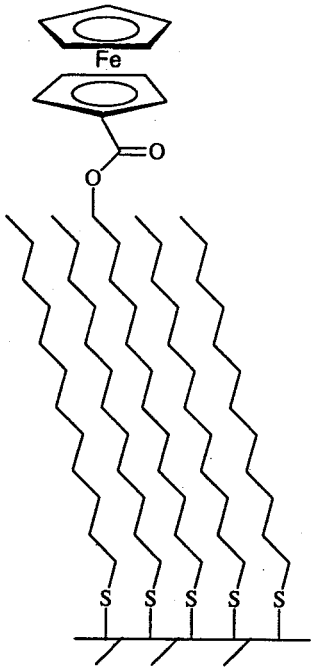

2. A/O

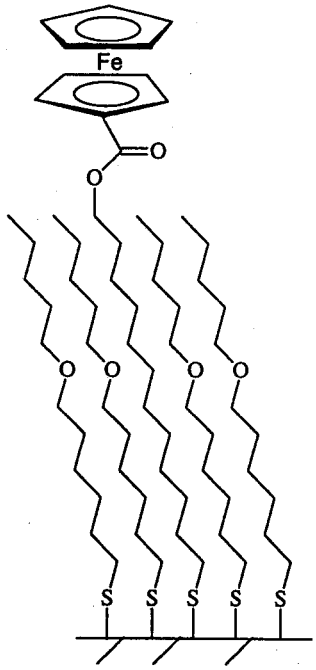

3. O/A

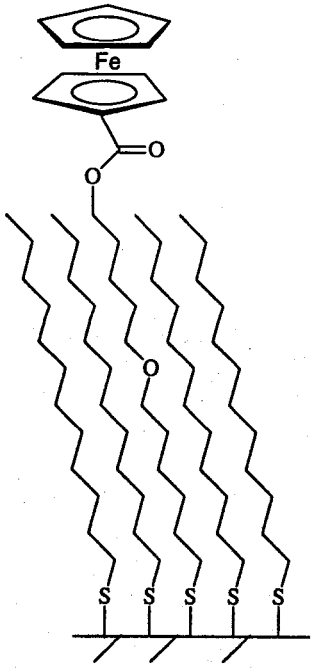

4. O/O

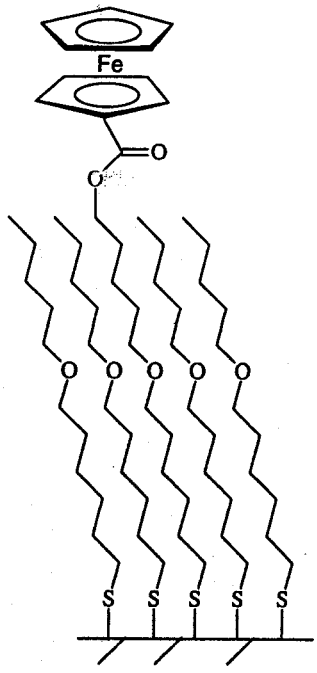

FIGURE 1

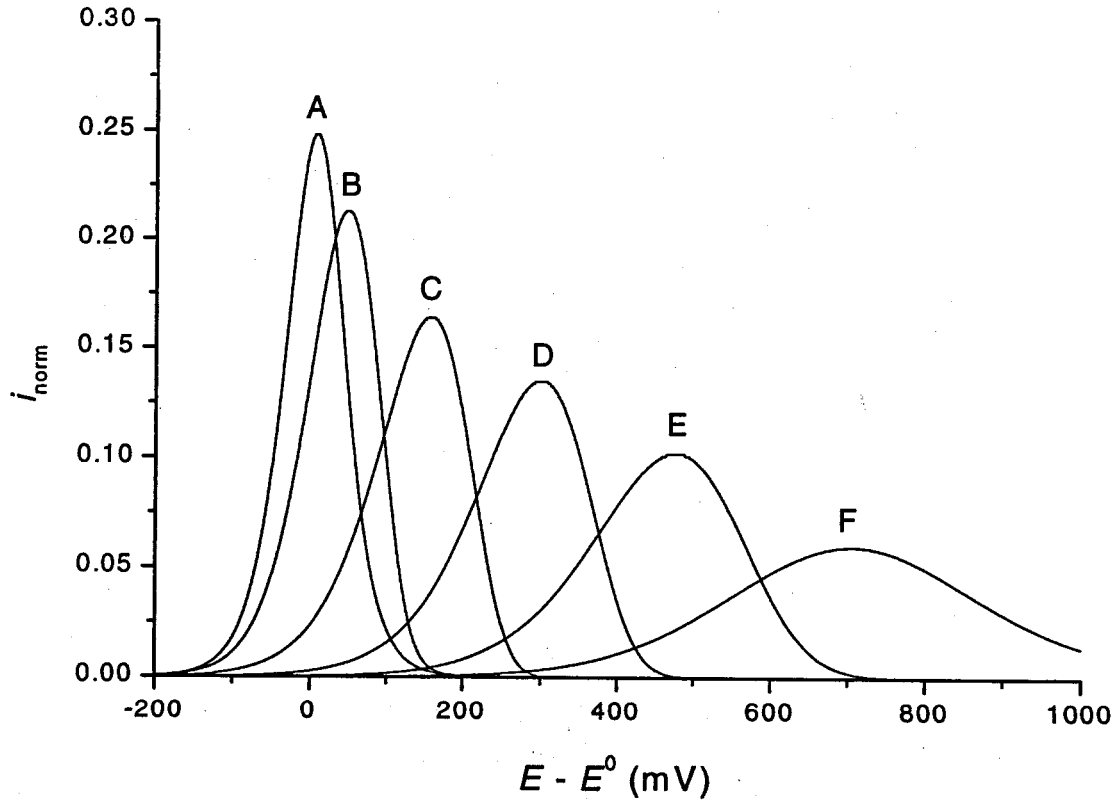
0.30
0.25
0.20
0.15
0.10
0.05
0.00
i_{norm}
A
B
C
D
E
F
-200
0
200
400
600
800
1000
$E - E^0$ (mV)

Figure 2

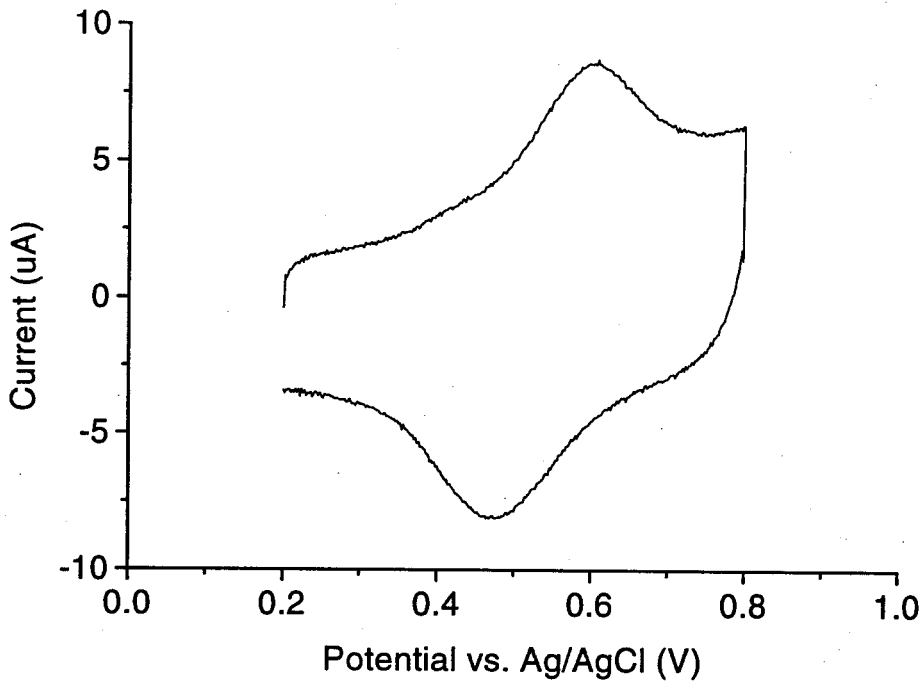

FIGURE 3

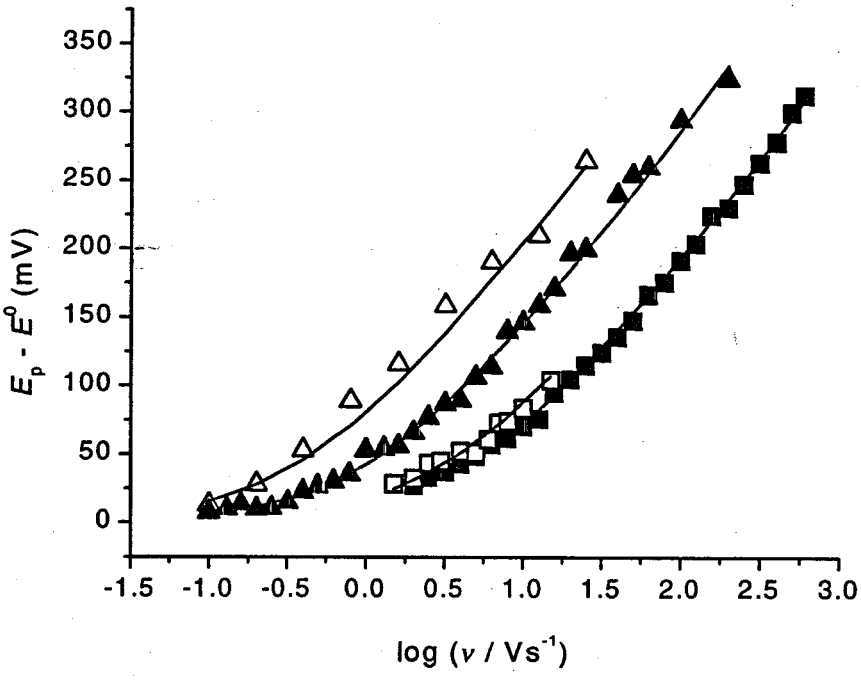
350
300
250
200
150
100
50
0
$E_p - E^0$ (mV)
-1.5
-1.0
-0.5
0.0
0.5
1.0
1.5
2.0
2.5
3.0
log (v / Vs^{-1})

Figure 4

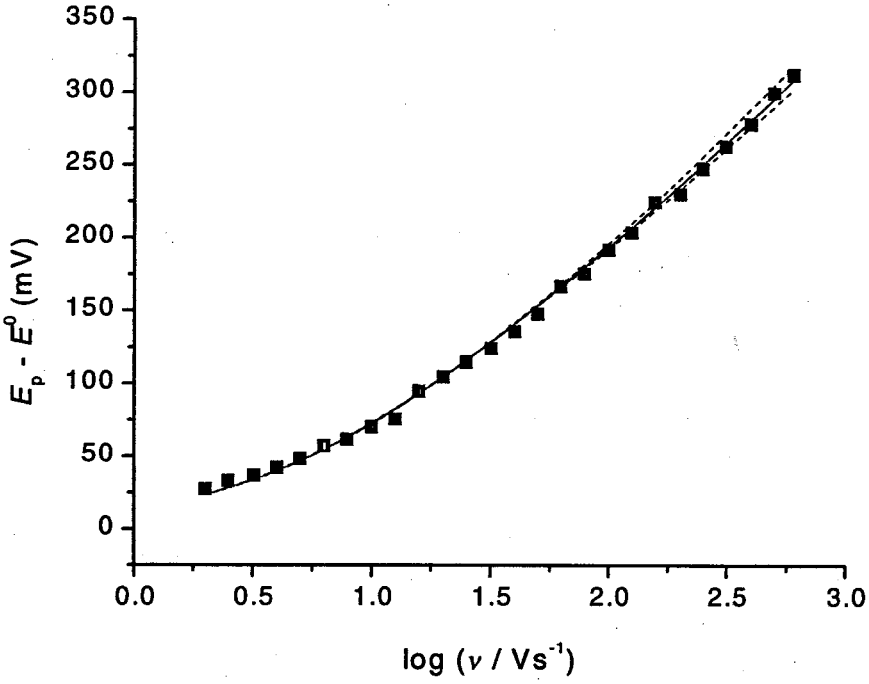

Figure 5

Figure 6

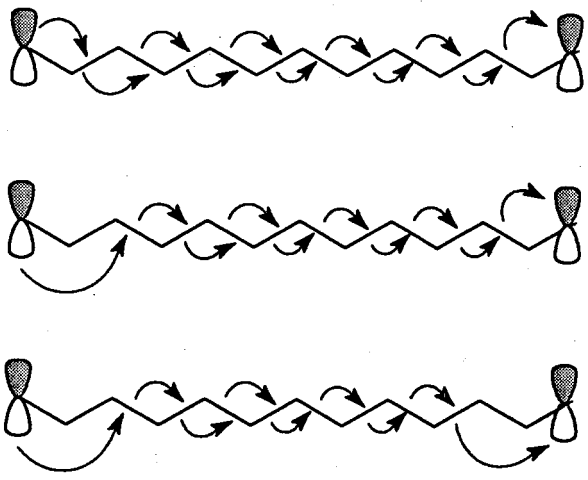

Figure 7

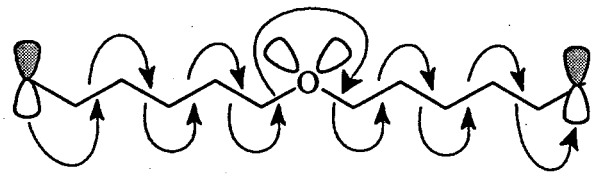

In Phase

$|V| = 0.120\ cm^{-1}$

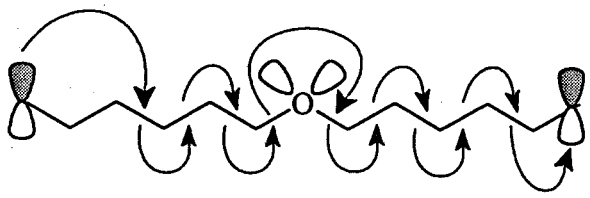

$|V| = 0.104\ cm^{-1}$

Out of Phase

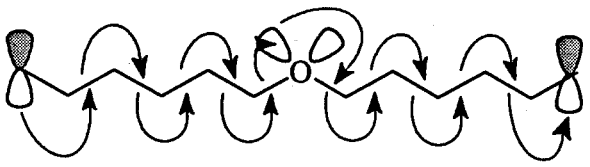

$|V| = 0.0955\ cm^{-1}$

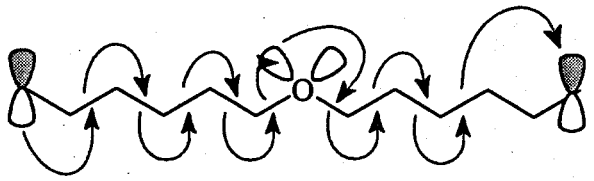

$|V| = 0.0827\ cm^{-1}$

Table 1. Kinetic Data for the Four Model Systems

Electroactive Thiol	Diluent Thiol	Rate Constant (s^{-1})	E^0 (mV vs. Ag/AgCl)	Number of Determinations
Alkane	Alkane	55.0 ± 9.1	522 ±13	10
Alkane	Ether	35 ± 12	532 ± 31	6
Ether	Alkane	12 ± 3	534 ± 13	3
Ether	Ether	8.4 ± 2.5	516 ± 32	7

The reported errors represent ± one standard deviation.

Table 2. Diagonalization of the NBO Fock matrices for the full bonding and antibonding manifolds of the two model diradicals.

Diradical	$\|V\|$ / cm^{-1} (Bonding)	$\|V\|$ / cm^{-1} (Antibonding)
$^{\bullet}CH_2(CH_2)_{11}CH_2^{\bullet}$	158	1.2
$^{\bullet}CH_2(CH_2)_5O(CH_2)_5CH_2$ $^{\bullet}$	86	1.4

Table 3. Electronic couplings calculated from NBO pathway calculations through the two model diradicals.

Diradical	$\|V\|$ / cm^{-1} (Bonding)	$\|V\|$ / cm^{-1} (In-Phase)	$\|V\|$ / cm^{-1} (Out-of-Phase)	$\|V_{in\text{-}phase}\| + \|V_{out\text{-}of\text{-}phase}\|$ / cm^{-1}
$^{\bullet}CH_2(CH_2)_{11}CH_2^{\bullet}$	43	43	0	43
$^{\bullet}CH_2(CH_2)_5O(CH_2)_5CH_2^{\bullet}$	25	37	12	49

REFERENCES

1 Liu, Yi-Ping; Newton, M. D. *J. Phys. Chem.* **1994**, 98, 7162-7169.

2 Newton, M. D. *J. Electroanal. Chem.* **1997**, 438, 3-10.

3 Gosavi, Shachi; Marcus, R. A. *J. Phys. Chem.* B; **2000**, 104, 2067-2072.

4 Forster, R. J.; Loughman, P.; Keyes, T. E. *J. Am. Chem. Soc.* **2000**, 122, 11948-11955.

5 Marcus, R. A.; Hsu, Chao-Ping *J. Chem. Phys.* **1997**, 106, 584-598.

6 Hsu, Chao-Ping *J. Electroanal. Chem.* **1997**, 438, 27-35.

7 a) A. Ulman *Characterization of Organic Thin Films*; Butterworth-Heinemann: Stoneham MA, **1995**. ; b) Ulman A. *An Introduction to Ultrathin Organic Films: From Langmuir- Blodgett to Self-Assembly*; Academic: Boston, **1991**.

8 Finklea, H. O. in *Electroanalytical Chemistry*, Bard, A. J., Rubinstein, I., Eds.; Marcel Dekker: New York, **1996**; Vol. 19, pp 109-335.

9 a) Chidsey, C. E. D *Science* **1991**, *251*, 919; b) Chidsey, C. E. D.; Bertozzi, C. R.; Putvinski, T. M.; Mujsce, A. M. *J. Am. Chem. Soc.* **1990**, *112*, 4301.

10 a) Weber, K.; Hockett, L.; Creager, S. *J. Phys. Chem. B* **1997**, *101*, 8286; b) Smalley, J. F.; Feldberg, S. W.; Chidsey, C. E. D.; Linford, M.R.; Newton, M. D.; Liu, Y. P. *J. Phys. Chem.* **1995**, *99*, 13141; c) Finklea, H. O.; Hanshew, D. D. *J. Am. Chem. Soc.* **1992**, *114*, 3174; d) Guo, L. H.; Facci, J. S.; McLendon, G. *J. Phys. Chem.* **1995**, *99*, 8458.

11 a) Gu, Y.; Waldeck, D. H. *J. Phys. Chem. B* **1998**, *102*, 9015; b) *ibid*, **1996**, *100*, 9573.

12 a) Creager, S.; Yu, C. J.; Bamdad, C.; O'Connor, S.; Maclean, T.; Lam, E.; Chong, Y.; Olsen, G. T.; Luo, J.; Gozin, M.; Kayyem, J. F. *J. Am. Chem. Soc.* **1999**, *121*, 1059; b) Sachs, S. B.; Dudek, S. P.; Hsung, R. P.; Sita, L. R.; Smalley, J. F.; Newton, M. D.; Feldberg, S. W.; Chidsey, C. E. D. *J. Am. Chem. Soc.* **1997**, *119*, 10563.

13 a) Finklea, H. O.; Ravenscroft, M. S. *Israel J. Chem.* **1997**, *37*, 179; b) Finklea, H. O.; Ravenscroft, M. S.; Snider, D. A. *Langmuir* **1993**, *9*, 223; c) Curtin, L. S.; Peck, S. R.; Tender, L. M.; Murray, R. W.; Rowe, G. K.; Creager, S. E. *Anal. Chem.* **1993**, *65*, 386; d) Richardson, J. N.; Peck. S. R.; Curtin, L. S.; Tender, L. M.; Terrill, R. H.; Carter, M. T.; Murray, R. W.; Rowe, G. K.; Creager, S. E. *J. Phys. Chem.* **1995**, *99*, 766.

14 a) Creager, S. E.; Rowe, G. K. *J. Electroanal. Chem.* **1997**, *420*, 291; b) Redpenning, J.; Flood, J. M. *Langmuir* **1996**, *12*, 508; c) Rowe, G. K.; Creager, S. E. *J. Phys. Chem.* **1994**, *98*, 5500; d) Creager, S. E.; Weber, K. *Langmuir* **1993**, *9*, 844; e) Fawcett, W. R. *J. Electroanal. Chem.* **1994**, *378*, 117.

15 Cruanes, M. T.; Drickamer, H. G.; Faulkner, L. R. *Langmuir* **1995**, *11*, 4089.

16 a) Carter, M. T.; Rowe, G. K.; Richardson, J. N.; Tender, L. M.; Terrill, R. H.; Murray, R. W. *J. Am. Chem. Soc.* **1995**, *117*, 2896; b) Richardson, J. N.; Rowe, G. K.; Carter, M. T.; Tender, L. M.; Curtin, S. C.; Peck, S. R.; Murray, R. W. *Electrochim. Acta.* **1995**, *40*, 1331; c) Rowe, G. K.; Carter, M. T.; Richardson J. N.; Murray, R. W. *Langmuir* **1995**, *11*, 1797.

17 Kumar, K.; Kurnikov, I. V.; Beratan, D. N.; Waldeck, D. H.; Zimmt, M. B. *J. Phys. Chem. A*, **1998**, 102, 5529-5541.

18 Kumar, K.; Lin, Z.; Waldeck, D. H.; Zimmt, M. B. *J. Am. Chem. Soc.* **1996**, 118, 243-244.

19 Ratner, M. A. *J. Phys. Chem.* **1990**, 94, 4877-4883.

20 Newton, M. D. *Chem. Rev.* **1991**, 91, 767-792.

21 a) Cheng, J.; Sàghi-Szabó, G.; Tossel, J. A.; Miller, C. J. *J. Am. Chem. Soc.* **1996**, 118, 680-684; b) Sinniah, K.; Cheng, J.; Terrettaz, S.; Reutt-Robey, J. E.; Miller, C. J. *J. Phys. Chem.* **1995**, *99*, 14500.

22 Sumner, J. J.; Weber, K. S.; Hockett, L. A.; Creager, S. E. *J. Phys. Chem B* **2000**, *104*, 7449.

23 a) Kergueris, C.; Bourgoin, J. P.; Palacin, S. *Nanotechnology* **1999**, *10*, 8; b) Kergueris, C.; Bourgoin, J. P.; Palacin, S.; Esteve, D.; Urbina, C.; Magoga, M.; Joachim, C. *Phys. Rev. B* **1999**, *59*, 12505; c) Tian, W.; Datta, S.; Hong, S.; Reifenberger, R.; Henderson, J. I.; Kubiak, C. P. *J. Chem. Phys.* **1998**, *109*, 2874; d) Samanta, M. P.; Tian, W.; Datta, S.; Henderson, J. I.; Kubiak, C. P. *Phys. Rev. B* **1996**, *95*, R7626.

24 a) Slowinski, K.; Chamberlain, R. V.; Majda, M.; Bilewicz, R. *J. Am. Chem. Soc.* **1996**, *118*, 4709; b) Slowinski, K.; Chamberlain, R. V.; Miller, C. J.; Majda, M. *J. Am. Chem. Soc.* **1997**, *119*, 11910-11919.

25 Finklea, H. O.; Liu, L.; Ravenscroft, M. S.; Punturi, S. *J. Phys. Chem.* **1996**, 100, 18852.

26 Sek, S.; Misicka, A.; Bilewicz, R. *J. Phys. Chem. B* **2000**, 104, 5399-5402.

27 Barbara, P.F.; Meyer, T. J.; Ratner, M. A. *J. Phys. Chem.* **1996**, *100*, 13148-13168.

28 a) Tender, L.; Carter, M. T.; Murray, R.W. *Anal. Chem.* **1994**, *66*, 3173; b) Weber, K.; Creager, S. E. *Anal. Chem.* **1994**, *66*, 3166; c) Honeychurch, M. J. *Langmuir* **1999**, *15*, 5158.

29 McConnell, H. M. *J. Chem. Phys.* **1961**, *35*, 508.

30 a) Gaussian 98, Revision A.9, M. J. Frisch, G. W. Trucks, H. B. Schlegel, G. E. Scuseria, M. A. Robb, J. R. Cheeseman, V. G. Zakrzewski, J. A. Montgomery, Jr., R. E. Stratmann, J. C. Burant, S. Dapprich, J. M. Millam, A. D. Daniels, K. N. Kudin, M. C. Strain, O. Farkas, J. Tomasi, V. Barone, M. Cossi, R. Cammi, B. Mennucci, C. Pomelli, C. Adamo, S. Clifford, J. Ochterski, G. A. Petersson, P. Y. Ayala, Q. Cui, K. Morokuma, D. K. Malick, A. D. Rabuck, K. Raghavachari, J. B. Foresman, J. Cioslowski, J. V. Ortiz, A. G. Baboul, B. B. Stefanov, G. Liu, A. Liashenko, P. Piskorz, I. Komaromi, R. Gomperts, R. L. Martin, D. J. Fox, T. Keith, M. A. Al-Laham, C. Y. Peng, A. Nanayakkara, M. Challacombe, P. M. W. Gill, B. Johnson, W. Chen, M. W. Wong, J. L. Andres, C. Gonzalez, M. Head-Gordon, E. S. Replogle, and J. A. Pople, Gaussian, Inc., Pittsburgh PA, **1998**; b) NBO Version 3.1, E. D. Glendening, A. E. Reed, J. E. Carpenter, and F. Weinhold.

31 a) Liang, C.; Newton, M. D. *J. Phys. Chem.* **1992**, 96, 2855-2866; b) Liang, C.; Newton, M. D. *J. Phys. Chem.* **1993**, 97, 3199-3211; c) Naleway, C. A.; Curtiss, L. A.; Miller, J. R. *J. Phys. Chem.* **1991**, 95, 8434-8437; d) Naleway, C. A.; Curtiss, L. A.; Miller, J. R. *J. Phys. Chem.* **1993**, 97, 4050-4058; e) Curtiss, L. A.; Naleway, C. A.; Miller, J. R. *Chem. Phys.* **1993**, 176, 387-405; f) Jordan K. D.; Paddon-Row, M. N.; "Electron Transfer Calculations", in *Encyclopedia of Comp. Chem.*, ed., P.V.R. Schleyer, **1998**, 2, 826; g) Jordan, K. D.; Nachtigallova, D.; Paddon-Row, M. N. in *Modern Electronic Structure Theory and Applications in Organic Chemistry*, ed. E.R. Davidson, World Scientific: Singapore, **1997**, 257.